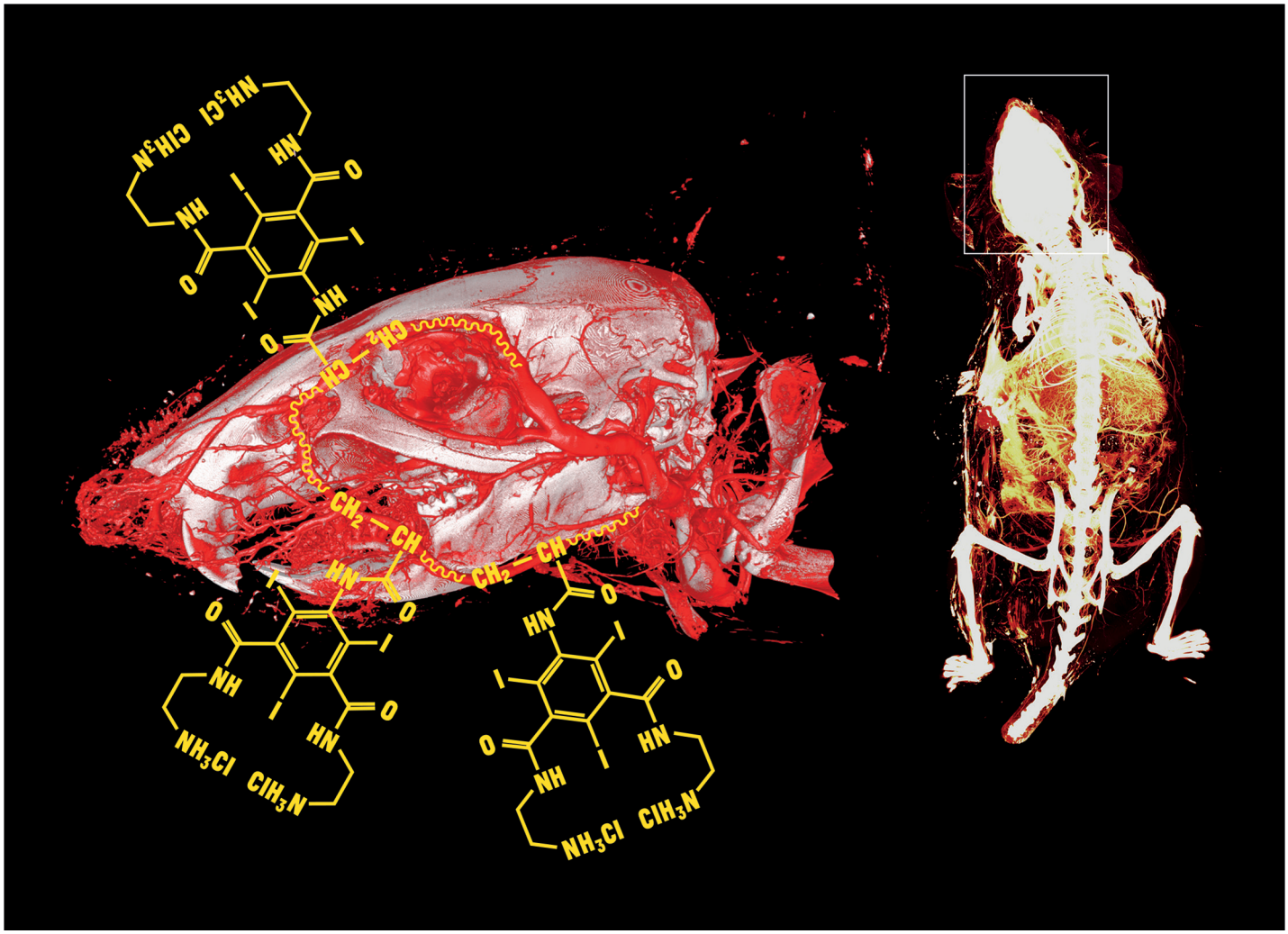

Showcasing research from the laboratories of Prof. Vartan Kurtcuoglu and Prof. Bernhard Spingler at the University of Zurich, Switzerland

Crosslinkable polymeric contrast agent for high-resolution X-ray imaging of the vascular system

The new, water soluble imaging agent *XlinCA* combines the simple and reliable perfusion of hydrophilic angiography contrast agents with the permanent retention and high contrast of hydrophobic vascular casting resins.

Image illustrated by Sarah Steinbacher, SIVIC, University of Zurich.

As featured in:

See Vartan Kurtcuoglu, Bernhard Spingler *et al.*, *Chem. Commun.*, 2020, **56**, 5885.

ROYAL SOCIETY OF CHEMISTRY

rsc.li/chemcomm

Registered charity number: 207890

ChemComm

COMMUNICATION

View Article Online
View Journal | View Issue

Cite this: *Chem. Commun.*, 2020, **56**, 5885

Received 23rd December 2019,
Accepted 27th April 2020

DOI: 10.1039/c9cc09883f

rsc.li/chemcomm

Crosslinkable polymeric contrast agent for high-resolution X-ray imaging of the vascular system†

Ngoc An Le, ‡[a] Willy Kuo, ‡[bcd] Bert Müller, [d] Vartan Kurtcuoglu *[bc] and Bernhard Spingler *[a]

A contrast agent for X-ray micro computed tomography (μCT), called *XlinCA*, that combines reliable perfusion and permanent retention and contrast properties, was developed for *ex vivo* imaging. The new imaging agent *XlinCA* features high molecular weight, low viscosity and a high iodine content.

Qualitative and quantitative assessment of vascular physiology, pathology and angiogenesis under various circumstances such as cancer, myocardial infarction, stroke, atherosclerosis, vasculitis, and inflammation requires accurate three-dimensional (3D) structural data.[1] A large number of different 3D imaging techniques can provide morphometric parameters including vessel volume, connectivity, number, thickness, thickness distribution, separation, and degree of anisotropy.[1b,d,2] These parameters are not only useful for investigating diseases that affect the vasculature, but are also crucial for proper evaluation of pro- and anti-angiogenic therapies in preclinical models.[3]

Micro computed tomography (μCT) allows for non-destructive 3D imaging with isotropic quality and micrometer resolution. The geometric magnification used in cone-beam μCT allows for continuously variable effective pixel sizes and for hierarchical imaging on low-resolution animal scale and high-resolution organ scale in a single device.[4] Whole small animals and organs can be imaged in their entirety in their native hydrated state, minimizing sample distortion through sample preparation artefacts, dehydration, realignment artefacts or optical distortion.

Ex vivo high-resolution X-ray imaging is not limited by movement during respiratory and cardiac cycles,[5] anaesthetic tolerance or the dose of ionizing radiation.[6] In addition, organs can be extracted and imaged at smaller fields of view, resulting in a corresponding increase of resolution in cone-beam μCT. The density difference between blood and soft tissue is, however, too small to be captured with standard absorption contrast using laboratory sources. Radiopaque X-ray contrast agents featuring heavy atomic elements have to be injected into the vasculature to provide the necessary contrast.[7]

Currently available contrast agents have various limitations when used for *ex vivo* vascular imaging. Standard clinical angiography contrast agents, such as iopamidol and iohexol, are small molecular compounds capable of passing through blood vessel walls, which also leads to a loss of contrast between the vascular lumen and the surrounding tissue within a few minutes.[8] This issue can be addressed by the use of blood pool contrast agents, which are large nanoparticles or polymeric compounds that can achieve vascular circulation times on the scale of hours.[9] In an *ex vivo* setting, blood pool contrast agents tend to sediment and aggregate, and can slowly leak out of the vasculature as well.[10] These limitations make both types of angiography contrast agents unsuitable for capillary resolution *ex vivo* vascular imaging.

For such application, the current gold standard consists of vascular casting with plastic resins, *e.g.* Microfil (Microfil, Flow Tech, Carver, MA), PU4ii (vasQtec, Zurich, Switzerland) and μAngiofil (Fumedica AG, Muri, Switzerland).[11] These hydrophobic resins are incapable of passing through the hydrated endothelial cell layer and polymerize after injection. They are thus permanently retained within the vasculature and provide excellent contrast. Perfusion of these resins is, however, technically challenging. The plastic resin may polymerize prematurely before the vasculature has been fully perfused, leading to incompletely filled blood vessels. Water inclusions and gas bubble formation are frequently occurring artefacts that cause disconnected vessel segments.[11a,12] Well-optimized injection techniques, closure of blood vessels *via* ligation in order to divert all flow to the organ of interest and high perfusion pressures are, therefore, required to obtain consistent perfusion results.[11a] While some of these problems can be attributed to the

[a] *Department of Chemistry, University of Zurich, 8057 Zurich, Switzerland. E-mail: spingler@chem.uzh.ch*
[b] *Institute of Physiology, University of Zurich, 8057 Zurich, Switzerland. E-mail: vartan.kurtcuoglu@uzh.ch*
[c] *National Centre of Competence in Research, Kidney.CH, 8057 Zurich, Switzerland*
[d] *Biomaterials Science Center, Department of Biomedical Engineering, University of Basel, 4123 Allschwil, Switzerland*

† Electronic supplementary information (ESI) available: Synthesis of *XlinCA* and further experimental details. See DOI: 10.1039/c9cc09883f

‡ These authors contributed equally to this work respectively.

high viscosity of the polymerizing plastic resins, they are inherent limitations shared by hydrophobic casting materials.

While plastic resins can provide reasonable vascular filling, extensive practice is required to reliably prevent frequent sample preparation failures and incomplete vessel filling.[13] Reliable vessel filling is, however, absolutely required for the quantitative characterization of pathological processes and the comparison of vascular phenotypes, as the resulting structural data is otherwise dominated by sample preparation artefacts and not representative of the true vascular structure.

In this paper, we address the shortcomings of current X-ray contrast agents in high resolution *ex vivo* imaging of the vascular network with μCT. We have developed a crosslinkable polymeric contrast agent, *XlinCA*, that combines the simple and reliable perfusion of the hydrophilic angiography contrast agents with the permanent retention and high contrast of the hydrophobic vascular casting resins. We demonstrate its application for capillary-level imaging of a brain hemisphere and vascular imaging of an entire mouse with a non-optimized transcardial perfusion. *XlinCA* was designed to fulfil a specific set of criteria to resolve issues encountered in *ex vivo* vascular imaging with current contrast agents:

- Highly water-soluble, so as to avoid incomplete vascular filling and interrupted vessel segments.

- Higher molecular weight than 65 kDa, for the prevention of immediate leakage through blood vessel walls.

- Crosslinkable with free primary amine groups as targets for glutaraldehyde fixation, which enables crosslinking *via* imine formation,[14] in order to prevent leakage over time.

- High X-ray attenuation coefficient with a high iodine content,[15] for reducing the required contrast agent concentration, viscosity and osmolarity.

After considering all the above criteria, we designed the crosslinkable polymeric contrast agent *XlinCA* represented schematically in Fig. 1. The theoretical iodine content is 49.5 m/m%, which is comparable to standard small molecule angiography iodine contrast agents and considerably higher than what could be achieved by other typical approaches, such as linkage to polyethylene glycol (PEG).[16]

The contrast agent was synthesized through a multi-step process, see Fig. S1 (ESI†). Starting from the commercially available 5-amino-2,4,6-triiodoisophthalic acid **1**, the acryloyl group was added through reaction with acrylic anhydride and a catalytic amount of sulfuric acid. The key step in this synthesis was the polymerization of **2** to give polymer **3** by reversible addition–fragmentation chain transfer (RAFT) polymerization.[17] Trithiocarbonate **7** was chosen as RAFT agent for polymerization of **2** due to the reported compatibility with various acrylamide derivatives.[18] We found that dimethylformamide (DMF) is the most suitable solvent for RAFT polymerization of **2**. It provides high solubility of both starting materials as well as polymeric products and allows a high degree of conversion of the monomers. The optimal reaction temperature was 70 °C. The concentrations of monomer, RAFT agent and AIBN as radical initiator were optimized (Table S2, ESI†). The average molecular weight of the synthesized polymer increases with the ratio of monomer to RAFT agent.[17d] The optimal ratio of monomer : RAFT agent : AIBN was found to be 400 : 2 : 1. Lower ratios of RAFT and AIBN to **2** led to higher conversion degrees, but lowered the molecular weight of **3**, while higher ratios led to precipitates of both starting material and product. The molecular weight of **3** could not be measured with gel permeation chromatography (GPC) even in warm DMF due to low solubility and the tendency of the polymer towards aggregation. However, the molecular weight and polydispersity index of **3** could be estimated indirectly from the GPC result of the final product **6**, which is water soluble and stable against aggregation. Based on the ratio of the molecular weights of the monomers and the average molecular weight of **6** (Fig. S6, ESI†), we calculated the average molecular weight of **3** to be 30 400 Da. Ethylenediamine was added to the polymer **3** after activation of the carboxylic groups with oxalyl chloride. The obtained **5** dissolved easily in dilute hydrochloric acid solution to give the contrast agent *XlinCA* (**6**), which is water soluble and can be crosslinked with aldehydes due to the presence of the amine groups.

The ability to be crosslinked not only enables polymerization of *XlinCA* after injection into the vasculature, but also facilitates the increase of the molecular weight of the contrast agent by pre-crosslinking with glutaraldehyde (Fig. S7, ESI†). In order to obtain the desired molecular weight of 65 kDa, required to prevent diffusion through the blood vessel walls, *XlinCA* was pre-crosslinked with different amounts of 25% glutaraldehyde prior to perfusion into the mouse. The highest amount that could be introduced without inducing gelation was found to be 30 μL of 25% glutaraldehyde solution per 1 g of *XlinCA* dissolved in 4 mL water. This ratio led to a limited increase in viscosity through an increase in the molecular weight of the polymer by pre-crosslinking. The pre-crosslinked contrast agent was dialysed with a 100 kDa dialysis membrane to remove all compounds below the size threshold and lyophilised. In this form it should be used within a week, as its solubility reduces over time. After the contrast agent was administered into the vasculature, further crosslinking of the contrast agent with glutaraldehyde led to gelation of the contrast agent, preventing any leakage and loss of contrast over time (Fig. S7, ESI†).

Mice perfused with vascular casting resin PU4ii and polymeric contrast agent *XlinCA* were compared by using low-resolution μCT with a voxel size of 80 μm. In the PU4ii-perfused mouse, numerous water inclusions and gas bubbles could be observed in the descending aorta, vena cava and larger vessels in the kidneys

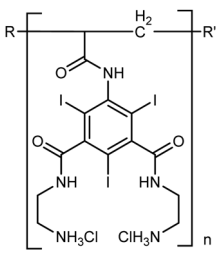

Fig. 1 Chemical formula of the crosslinkable polymeric X-ray contrast agent *XlinCA*.

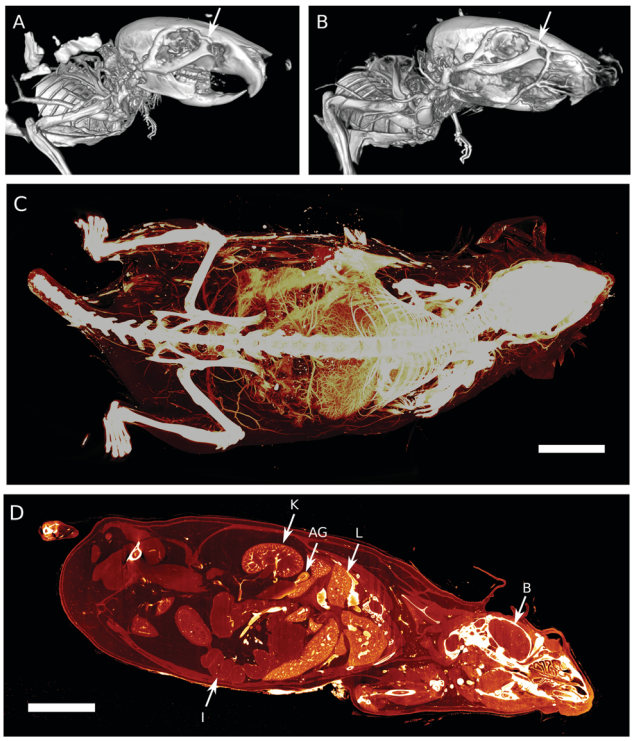

Fig. 2 Conventional μCT images of mouse heads perfused with PU4ii (A) and *XlinCA* (B). In the PU4ii-filled mouse, the supraorbital vein (white arrow) is partially filled up to the bifurcation to the naso-frontal vein and anterior facial vein, which do not appear. In contrast, these vessels, along with the anterior facial vein, are completely filled in the *XlinCA*-perfused mouse. (C) Maximum intensity projection of the higher resolution *XlinCA*-perfused whole mouse dataset. Voxel size: 20 μm, scale bar: 1 cm. (D) Virtual section of the μCT dataset shown in (C). Intestine (I), kidney (K), adrenal gland (AG), liver (L) and brain (B) are clearly visible. Scale bar: 1 cm.

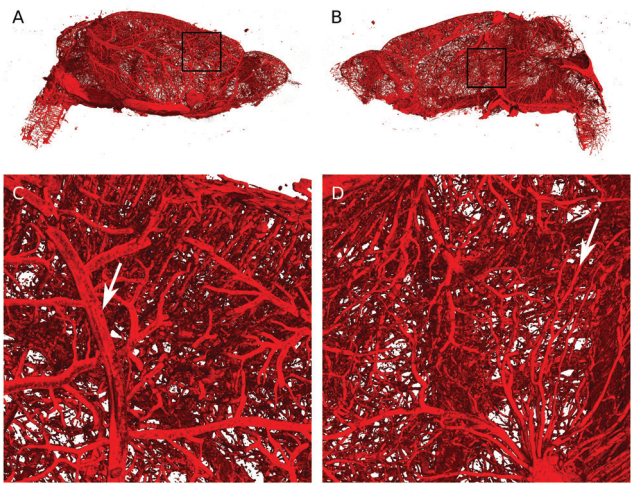

Fig. 3 3D rendering of the brain hemisphere vasculature perfused with *XlinCA*. (A) Outside view. (B) Inside view. (C) Magnified view of the region indicated by the black square in (A). Diameter of blood vessel indicated by the white arrow: 70 μm. (D) Magnified view of (B). Diameter of blood vessel indicated by the white arrow: 15 μm.

and the liver. Correspondingly, one liver lobe, the adrenal glands and part of the kidneys were only partially filled with PU4ii. Certain large blood vessels, such as the naso-frontal vein and anterior vein, remained completely devoid of PU4ii (Fig. 2A), while their counterparts in the mouse perfused with *XlinCA* were filled in their entirety (Fig. 2B and Fig. S8, ESI†). In order to evaluate completeness of the vessel filling further, the *XlinCA*-perfused mouse was scanned with a voxel size of 20 μm. Brain, heart, lungs, liver, kidneys and adrenal glands appeared well-perfused, see Fig. 2C, D and Fig. S9, S10 (ESI†). No discontinuous vessel segments could be found, as expected for a water-soluble compound. Vascular filling with *XlinCA* was not entirely complete. Small vessels posterior to the kidneys were ill-defined. Parts of the capillaries were missing in the renal medulla of the kidney (Fig. S10, ESI†) and the spleen. Leftover blood seen in the histological examination indicated that this was caused by incomplete flushing of blood prior to contrast agent injection, and thus not due to any contrast agent-related property.

The brain of the *XlinCA*-perfused mouse was removed and the right brain hemisphere was scanned with a voxel size of 4.4 μm, as the smaller field of view allowed for scans with approximately twice the resolution compared to a full brain. There were no large areas of missing vasculature as has been reported for optimized Microfil perfusions.[11a] Neither vessel discontinuities through insufficient filling nor gas bubbles could be identified (Fig. 3). Independent of the choice of vascular casting agent, non-optimized transcardial perfusion techniques cannot entirely outperform optimized perfusion techniques in specific organs. On equal terms, however, *XlinCA* provided more complete and reliable filling of multiple organs in an entire mouse with a simple transcardial injection, without requiring clamping or ligation of the descending aorta and vena cava (Fig. S11, ESI†). The procedure is thus much simpler to perform and allows multiple organs to be harvested and used in the analysis of the vasculature, which reduces the number of animals required and the variance in multi-organ correlation studies.

Factors such as injection volume and flow rate did not have to be optimized, as crosslinking can be initiated at any time after perfusion is complete. In contrast, Microfil polymerizes within approximately 20 minutes,[11a] limiting the perfusion volume before viscosity and thus resistance to flow increases. With the time constraints removed, flow rate and thus perfusion pressure are no longer factors that require optimization. Perfusion pressure in our experiment was 150 mmHg, which is consistent with the pressure used in the transcardial perfusion reported by Chugh *et al.*,[12b] but lower pressures can be used without risk of premature polymerization and resulting incomplete filling. Higher perfusion pressures are still of advantage in the prior perfusion steps required for flushing the vasculature of remaining blood, however.

In conclusion, we have shown that our new imaging agent *XlinCA* circumvents the limitations of current vascular casting with plastic resins. As *XlinCA* is a water-soluble compound, water inclusions are inherently avoided. The contrast agent is free of microparticles, thereby preventing blockage of capillaries by solid aggregates. Crosslinking can be initiated after perfusion is complete, allowing perfusion to be conducted for any desired period of time without an increase in viscosity limiting the

amount of contrast agent volume that can be injected. The flow rate does not need optimization, and perfusion pressure ceases to be an important factor for contrast agent filling.

Vascular casting with *XlinCA* thus requires not only considerably less technical expertise and time, but also permits perfusion of both the brain and the whole mouse in a single procedure. We envision that these features will enable hierarchical imaging of organs in their original spatial context and identification of areas with vascular abnormalities, which can then be excised for higher resolution imaging. The vasculature of more than one organ of the same animal could be analysed, which would reduce the number of animals required and reduce the variance in multi-organ correlation studies.

This work was financially supported by University of Zurich and the Swiss National Science Foundation through NCCR Kidney.CH, R'Equip 133802 and grant 205321_153523. We thank Dr Thomas Fox for recording the ^{1}H-NMR of *XlinCA* (**6**) and Dr Georg Schulz for support for the high resolution μCT scans.

Conflicts of interest

A patent application for the polymeric contrast agent described in this publication has been filed by the University of Zurich.

References

1 (*a*) Z. Starosolski, C. A. Villamizar, D. Rendon, M. J. Paldino, D. M. Milewicz, K. B. Ghaghada and A. V. Annapragada, *Sci. Rep.*, 2015, **5**, 10178; (*b*) J. Ehling, J. Babickova, F. Gremse, B. M. Klinkhammer, S. Baetke, R. Knuechel, F. Kiessling, J. Floege, T. Lammers and P. Boor, *J. Am. Soc. Nephrol.*, 2016, **27**, 520–532; (*c*) J. López-Guimet, L. Peña-Perez, R. S. Bradley, P. Garcia-Canadilla, C. Disney, H. Geng, A. J. Bodey, P. J. Withers, B. Bijnens, M. J. Sherratt and G. Egea, *Theranostics*, 2018, **8**, 6038–6052; (*d*) J. Epah, K. Palfi, F. L. Dienst, P. F. Malacarne, R. Bremer, M. Salamon, S. Kumar, H. Jo, C. Schürmann and R. P. Brandes, *Theranostics*, 2018, **8**, 2117–2133.

2 L. Zagorchev, P. Oses, Z. W. Zhuang, K. Moodie, M. J. Mulligan-Kehoe, M. Simons and T. Couffinhal, *J. Angiogenes Res.*, 2010, **2**, 7.

3 (*a*) J. Ehling, B. Theek, F. Gremse, S. Baetke, D. Mockel, J. Maynard, S. A. Ricketts, H. Grull, M. Neeman, R. Knuechel, W. Lederle, F. Kiessling and T. Lammers, *Am. J. Pathol.*, 2014, **184**, 431–441; (*b*) L. Ayala-Dominguez and M. E. Brandan, *Biomed. Phys. Eng. Express*, 2018, **4**, 062001; (*c*) S. Gu, J. Xue, Y. Xi, R. Tang, W. Jin, J.-J. Chen, X. Zhang, Z.-M. Shao and J. Wu, *Quant. Imaging Med. Surg.*, 2019, **9**, 418–426.

4 (*a*) L. A. Walton, R. S. Bradley, P. J. Withers, V. L. Newton, R. E. B. Watson, C. Austin and M. J. Sherratt, *Sci. Rep.*, 2015, **5**, 10074; (*b*) E. L. Ritman, *Proc. SPIE*, 2011, **7898**, 78980I; (*c*) T. Salditt, T. Aspelmeier and S. Aeffner, *Biomedical Imaging: Principles of Radiography, Tomography and Medical Physics*, De Gruyter, Berlin, Boston, 1st edn, 2017.

5 R. J. Alfidi, W. J. Mac Intyre and J. R. Haaga, *Am. J. Roentgenol.*, 1976, **127**, 11–15.

6 (*a*) J. Lerch, L. Gazdzinski, J. Germann, J. Sled, R. M. Henkelman and B. Nieman, *Front. Neuroinform.*, 2012, **6**, 6; (*b*) S. K. Carlson, K. L. Classic, C. E. Bender and S. J. Russell, *Mol. Imaging Biol.*, 2007, **9**, 78–82.

7 (*a*) B. Müller, J. Fischer, U. Dietz, P. J. Thurner and F. Beckmann, *Nucl. Instrum. Methods Phys. Res., Sect. B*, 2006, **246**, 254–261; (*b*) E. Eggl, K. Mechlem, E. Braig, S. Kulpe, M. Dierolf, B. Günther, K. Achterhold, J. Herzen, B. Gleich, E. Rummeny, P. B. Noël, F. Pfeiffer and D. Muenzel, *Sci. Rep.*, 2017, **7**, 42211.

8 M. Bourin, P. Jolliet and F. Ballereau, *Clin. Pharmacokinet.*, 1997, **32**, 180–193.

9 (*a*) F. Hallouard, N. Anton, P. Choquet, A. Constantinesco and T. Vandamme, *Biomaterials*, 2010, **31**, 6249–6268; (*b*) L. Nebuloni, G. A. Kuhn and R. Müller, *Acad. Radiol.*, 2013, **20**, 1247–1255; (*c*) C. Gao, Y. Zhang, Y. Zhang, S. Li, X. Yang, Y. Chen, J. Fu, Y. Wang and X. Yang, *Polym. Chem.*, 2020, **11**, 889–899.

10 W. Kuo, G. Schulz, B. Müller and V. Kurtcuoglu, *Developments in X-Ray Tomography XII*, San Diego, California, USA, 2019, p. 111130Q.

11 (*a*) S. Ghanavati, L. X. Yu, J. P. Lerch and J. G. Sled, *J. Neurosci. Meth.*, 2014, **221**, 70–77; (*b*) T. Krucker, A. Lang and E. P. Meyer, *Microsc. Res. Tech.*, 2006, **69**, 138–147; (*c*) L. Schaad, R. Hlushchuk, S. Barre, R. Gianni-Barrera, D. Haberthur, A. Banfi and V. Djonov, *Sci. Rep.*, 2017, **7**, 41842.

12 (*a*) S. Grabherr, V. Djonov, K. Yen, M. J. Thali and R. Dirnhofer, *Am. J. Roentgenol.*, 2007, **188**, 832–838; (*b*) B. P. Chugh, J. P. Lerch, L. X. Yu, M. Pienkowski, R. V. Harrison, R. M. Henkelman and J. G. Sled, *NeuroImage*, 2009, **47**, 1312–1318; (*c*) S. X. Vasquez, F. Gao, F. Su, V. Grijalva, J. Pope, B. Martin, J. Stinstra, M. Masner, N. Shah, D. M. Weinstein, R. Farias-Eisner and S. T. Reddy, *PLoS One*, 2011, **6**, e19099; (*d*) L. Fan, S. Wang, X. He, E. Gonzalez-Fernandez, C. Lechene, F. Fan and R. J. Roman, *Physiol. Rep.*, 2019, **7**, e14065.

13 D. S. Perrien, M. A. Saleh, K. Takahashi, M. S. Madhur, D. G. Harrison, R. C. Harris and T. Takahashi, *BMC Nephrol.*, 2016, **17**, 24.

14 (*a*) D. T. Cheung and M. E. Nimni, *Connect. Tissue Res.*, 1982, **10**, 187–199; (*b*) I. Migneault, C. Dartiguenave, M. J. Bertrand and K. C. Waldron, *Biotechniques*, 2004, **37**, 790–802.

15 H. Lusic and M. W. Grinstaff, *Chem. Rev.*, 2013, **113**, 1641–1666.

16 E. Jin and Z.-R. Lu, *Biomaterials*, 2014, **35**, 5822–5829.

17 (*a*) J. Chiefari, Y. K. Chong, F. Ercole, J. Krstina, J. Jeffery, T. P. T. Le, R. T. A. Mayadunne, G. F. Meijs, C. L. Moad, G. Moad, E. Rizzardo and S. H. Thang, *Macromolecules*, 1998, **31**, 5559–5562; (*b*) C. Boyer, V. Bulmus, T. P. Davis, V. Ladmiral, J. Liu and S. Perrier, *Chem. Rev.*, 2009, **109**, 5402–5436; (*c*) D. J. Keddie, *Chem. Soc. Rev.*, 2014, **43**, 496–505; (*d*) S. Perrier, *Macromolecules*, 2017, **50**, 7433–7447.

18 G. Moad, E. Rizzardo and S. H. Thang, *Aust. J. Chem.*, 2012, **65**, 985–1076.

